Asian Journal of Chemistry; Vol. 25, No. 14 (2013), 7687-7696

ASIAN JOURNAL OF CHEMISTRY

http://dx.doi.org/10.14233/ajchem.2013.14571

Dissolution and Solubility of the Erythrite/Annabergite Solid Solution $[(Co_xNi_{1-x})_3(AsO_4)_2 \cdot 8H_2O]$ at 25 ºC

CAICHUN WEI[1,2], YINIAN ZHU[2,*], XUEHONG ZHANG[2], XIAOMING WANG[2] and JIE LIU[2]

[1]College of Light Industry and Food Engineering, Guangxi University, Nanning 530004, Guangxi Province, P.R. China
[2]College of Environmental Science and Engineering, Guilin University of Technology, Jian-Gan Road 12, Guilin 541004, P.R. China

*Corresponding author: Fax: +86 773 5895330; Tel: +86 773 5897016; E-mail: zhuyinian@163.com

(*Received*: 14 September 2012; *Accepted*: 8 July 2013) AJC-13788

Nine different members of the erythrite/annabergite solid solution $[(Co_xNi_{1-x})_3(AsO_4)_2 \cdot 8H_2O]$ were prepared and characterized by various techniques and then dissolution of the synthetic solids was studied at 25 ºC and pH 2 in a series of batch experiments for 2880 h. The result indicated that the erythrite/annabergite solid solution had a minimum aqueous arsenate concentration or a minimum solubility at the mole fraction of erythrite in the solid solution of x = 0.70. The Guggenheim parameters a_o and a_1 were determined to be -1.79 and 1.23 from the alyotropic composition and alyotropic solubility at x = 0.70. A Lippmann diagram for the ideal case when $a_0 = 0.0$ and for the non-ideal case when $a_0 = -1.79$ and $a_1 = 1.23$ was constructed using the thermodynamic solubility products for erythrite of $10^{-33.68}$ and annabergite of $10^{-32.34}$. The experimental data were plotted on Lippmann phase diagrams to show the evolution of the aqueous composition during the dissolution of the erythrite/annabergite solid solution.

Key Words: Erythrite, Annabergite, Solid solution, Dissolution, Solubility.

INTRODUCTION

Arsenic has been known from antiquity to be highly toxic for animals and the majority of plants[1]. Mining activities are often associated with significantly increased arsenic concentrations in mine water. Arsenic toxicity is a global health problem affecting many millions of people[2]. Occurrences of dissolved arsenic in surface and ground waters and observed adverse health effects have emphasized the need for better understanding of reactions that govern arsenic mobility in the environment[3]. It is possible that removal of As(V) is enhanced by synergistic co-precipitation with other cationic metals in the formation of a arsenate mineral phase or phases. Recovery of arsenic as precipitate of natural mineral from arsenic-containing wastewaters was investigated by hydrothermal mineralization treatment[4,5].

Secondary minerals may form in a variety of ways within the zone of sulfide mineral oxidation in mine-waste systems and are of particular interest in mine-waste systems because they act as solid-phase controls on aqueous-species concentrations in the pore water. The migration of metallic contaminants to the surrounding environment with flowing pore water is one of the principal concerns in the management of mine-waste materials, characterization of secondary minerals can lead to a better assessment of the long-term impact of the mine waste[6,7]. A large number of secondary arsenate minerals have been found in highly contaminated soils, stream sediments, former industrial sites and mine tailings[8]. The ability of secondary arsenate minerals to immobilize arsenic and control its dissolved concentrations depends on the solubility of these phases, which is highly variable[8]. Some deposits, such as hydrothermal five-element associations and many uranium deposits, contain Ni-Co-Fe arsenides and sulfur-senides. The oxidation of these primary arsenic minerals typically leads to the formation of greenish and pinkish secondary compounds, annabergite and erythrite, respectively. The precipitation of erythrite has been expected to exert significant, if not dominant, control over the dissolved concentrations of Co and As and probably over the concentrations of Ni, which substitutes for Co forms a erythrite/annabergite solid solution $[(Co_xNi_{1-x})_3(AsO_4)_2 \cdot 8H_2O]$[6,8-11].

Solid solutions are geochemically and environmentally important because the interaction of dissolved toxic metals with minerals frequently results in the precipitation of metal-bearing solid solutions on the mineral surfaces or in rock or sediment pores. As a result, metals can be removed from natural waters and the thermodynamic properties of these solid solutions have a vital influence on the transport and fate of toxic metals in the environment[12]. Physico-chemical and electronic properties of minerals are often highly dependent on the composition of solid solutions. These properties are typically not a linear function of the mole fractions of the end-members.

Therefore, the science of solid solutions is a growing field within the material, earth and environmental sciences[12]. Only a few studies have been carried out on the erythrite/annabergite solid solution, especially on its dissolution and stability, for which little information exists in the literature. Consequently, there are insufficient data upon which to assess the true environmental risk of arsenic, cobalt and nickel posed by these minerals.

In the present study, a series of the erythrite/annabergite solid solution [$(Co_xNi_{1-x})_3(AsO_4)_2{\cdot}8H_2O$] with different Co/(Co + Ni) atomic ratios were prepared by a precipitation method. The resulting solid solution particles were characterized by various techniques. This paper reports the results of a study that monitors the dissolution and release of constituent elements from synthetic erythrite/annabergite solid solutions using batch dissolution experiments. The solid-solution aqueous-solution reaction paths are also discussed using the Lippmann diagram to evaluate the potential impact of such solid-solutions on the mobility of arsenic in the environment.

EXPERIMENTAL

Solid preparation and characterization: The experimental details for the preparation of the samples by precipitation were based on the following equation: $3X^{2+}+2AsO_4^{3-}+8H_2O = X_3(AsO_4)_2{\cdot}8H_2O$. Where $X = Co^{2+}$ or Ni^{2+}. The erythrite/annabergite solid solutions [$(Co_xNi_{1-x})_3(AsO_4)_2{\cdot}8H_2O$] were synthesized by controlled mixing of a solution of 66.67 mL of 0.5 M Na_3AsO_4 and a solution of 100 mL 0.5 M $Co(C_2H_3O_2)_2$ and $Ni(CH_3COO)_2$, so that the (Co+Ni)/As molar ratio in the mixed solution was 1.50. Reagent grade chemicals and ultrapure water were used for the synthesis and all experiments. The amounts of $Co(CH_3COO)_2$ and $Ni(CH_3COO)_2$ were varied in individual syntheses to obtain synthetic solids with different mole fractions of $Co_3(AsO_4)_2{\cdot}8H_2O$ (Table-1). The initial solutions were slowly mixed in a covered beaker in a course of 10 min at room temperature (23 ± 1 ºC). The resulting solution was kept at 70 ºC and stirred at a moderate rate (100 rpm) using a stirrbar. After a week, the precipitates were allowed to settle. The resultant precipitates were then washed thoroughly with ultrapure water and dried at 110 ºC for 24 h.

The composition of the sample was determined. The residual Co, Ni and As concentrations in the decanted solutions were analyzed to calculate the compositions of the precipitates. In addition, approximately 10 mg of sample was digested in 20 mL of 1 M HNO_3 solution and then diluted to 100 mL with ultrapure water. It was analyzed for Co, Ni and As using a Perkin Elmer Model AAnalyst 700 atomic absorption spectrometer (AAS). The detection limits of graphite furnace atomic adsorption for Co, Ni and As were 0.15, 0.07 and 0.05 µg/L with the estimated standard deviations of 2, 2 and 5 %, respectively. The synthetic solids were characterized by powder X-ray diffraction with an X'Pert PRO diffractometer using CuK_α radiation (40 kV and 40 mA). Crystallographic identification of the synthesized solid was accomplished by comparing the experimental XRD pattern to standard compiled by the international centre for diffraction data (ICDD), which were card 00-033-0413 for erythrite and card 00-034-0141 for annabergite. The morphology was analyzed by scanning electron microscopy (SEM, Joel JSM-6380LV). Infrared transmission spectra (KBr) were recorded over the range of 4000-400 cm^{-1} using a Fourier transformed infrared spectrophotometer (FT-IR, Nicolet Nexus 470 FT-IR).

Dissolution experiments: 1 g of the synthetic solid was placed in 250 mL polypropylene bottle. 150 mL of 0.01 M HNO_3, ultrapure water or 10^{-5} M NaOH solution was added into each bottle. The bottles were capped and placed in a temperature-controlled water bath (25 ºC). Water samples (3 mL) were taken from each bottle on 18 occasions (1 h, 3 h, 6 h, 12 h, 1 d, 2 d, 3 d, 5 d, 10 d, 15 d, 20 d, 30 d, 40 d, 50 d, 60 d, 75 d, 90 d, 120 d). After each sampling, the sample volume was replaced with an equivalent amount of ultrapure water. The samples were filtered using 0.20 µm pore diameter membrane filters and stabilized with 0.2 % HNO_3 in 25 mL volumetric flask. Co, Ni and As were analyzed by using an atomic absorption spectrometer (Perkin Elmer Model AAnalyst 700). After 120d of dissolution, the solid samples were taken from each bottle, washed, dried and characterized using XRD, SEM and FT-IR in the same manner as described above. All further tests were done using nitrate media to minimize the precipitation of impurity phases and to prevent the complexation of the metal ions at higher concentration.

Thermodynamic calculations: Associated with each dissolution is an assemblage of solid phases, a solution phase containing dissolved cobalt, nickel and arsenate and a pH value. Assuming equilibrium has been reached, the thermodynamic data can be calculated using established theoretical principles[13,14]. In this study, the simulations were performed using PHREEQC (Version 2.18) together with the modified minteq.v4.dat database, which bases on the ion dissociation theory. The input is free-format and uses order-independent keyword data blocks that facilitate the building of models that can simulate a wide variety of aqueous-based scenarios[15]. The activities of Co^{2+}(aq), Ni^{2+}(aq) and AsO_4^{3-}(aq) were calculated by using PHREEQC. The saturation indexes were also calculated with respect to erythrite and annabergite. The thermodynamic constants of the metal arsenate complexes were estimated by Marini and Accornero[16,17].

RESULTS AND DISCUSSION

Solid characterizations: The composition of the synthetic solid depends on the initial Co:Ni:As mole ratio in the starting solution. To ensure that the erythrite/annabergite solid solution was formed, the precipitation was conducted by mixing cobalt solution, nickel solution and arsenate solution at low rate. Results suggest that the crystal was the intended composition of $(Co_xNi_{1-x})_3(AsO_4)_2{\cdot}8H_2O$. The atomic (Co + Ni)/As ratio was 1.50 which is a stoichiometric ratio of erythrite and annabergite. No Na^+ and NO_3^- were detected in the prepared solid (Table-1).

XRD, FT-IR and SEM analyses were performed on the solids before and after the dissolution experiments (Figs. 1-3). As illustrated in the figures, the results of the analyses on materials before the dissolution were almost indistinguishable from the following reaction. No evidence of secondary mineral precipitation was observed in the dissolution experiment.

The XRD patterns of the obtained solids indicated the formation of the $(Co_xNi_{1-x})_3(AsO_4)_2{\cdot}8H_2O$ solid solution, which

TABLE-1
SYNTHESIS AND COMPOSITION OF THE NINE TYPES OF $(Co_xNi_{1-x})_3(AsO_4)_2{\cdot}8H_2O$ SOLID SOLUTION

Sample no.	Volumes of the precursors (mL)			Solid composition
	0.5 M $Co(C_2H_3O_2)_2$	0.5 M $Ni(C_2H_3O_2)_2$	0.5 M Na_3AsO_4	
EryAnna-1	90	10	66.67	$(Co_{0.9}Ni_{0.1})_3(AsO_4)_2{\cdot}8H_2O$
EryAnna-2	80	20	66.67	$(Co_{0.8}Ni_{0.2})_3(AsO_4)_2{\cdot}8H_2O$
EryAnna-3	70	30	66.67	$(Co_{0.7}Ni_{0.3})_3(AsO_4)_2{\cdot}8H_2O$
EryAnna-4	60	40	66.67	$(Co_{0.6}N_{i0.4})_3(AsO_4)_2{\cdot}8H_2O$
EryAnna-5	50	50	66.67	$(Co_{0.5}Ni_{0.5})_3(AsO_4)_2{\cdot}8H_2O$
EryAnna-6	40	60	66.67	$(Co_{0.4}Ni_{0.6})_3(AsO_4)_2{\cdot}8H_2O$
EryAnna-7	30	70	66.67	$(Co_{0.3}Ni_{0.7})_3(AsO_4)_2{\cdot}8H_2O$
EryAnna-8	20	80	66.67	$(Co_{0.2}Ni_{0.8})_3(AsO_4)_2{\cdot}8H_2O$
EryAnna-9	10	90	66.67	$(Co_{0.1}Ni_{0.9})_3(AsO_4)_2{\cdot}8H_2O$

has the same type of structure as erythrite and annabergite (Fig. 1). The patterns correspond exactly with the database patterns and no impurities are observed. The solid solution is complete, with the space group C2/m (monoclinic) being retained throughout[18]. Erythrite and annabergite are the two endmembers of a structural family series. When subjected to XRD, they produce the same reflections; but the reflections exist at different 2θ values, *i.e.*, the reflective planes are the same but "d" spacings are different. All the compounds have indicated the formation of a solid phase differing only in reflection location, reflection width and absolute intensity of the diffraction patterns. The reflection peaks of erythrite and annabergite were slightly different from each other. The reflections of the $(Co_xNi_{1-x})_3(AsO_4)_2{\cdot}8H_2O$ solid solutions shifted gradually to a higher-angle direction when the mole fraction of $Co_3(AsO_4)_2{\cdot}8H_2O$ of the solids decreased (Fig. 1).

The FT-IR spectra of the erythrite/annabergite solid solutions are shown in Fig. 2. The spectra may be divided into three sections: (a) hydroxyl-stretching region (b) water HOH bending region and (c) arsenate As-O stretching and OAsO bending region. The free arsenate ion, AsO_4^{3-}, belongs to the point group T_d. The normal modes of the tetrahedral arsenate ion are: ν_1, symmetric As-O stretching; ν_2, OAsO bending; ν_3, As-O stretching and ν_4, OAsO bending. In the undistorted state, only the absorptions corresponding to ν_3 and ν_4 vibrations are observed. The two remaining fundamentals ν_1 and ν_2 become infrared active when the configuration of the AsO_4^{3-} ions is reduced to some lower symmetry[19]. The degenerate modes are split by distortion of the arsenate groups through lack of symmetry in the lattice sites. As shown in Fig. 2, the peaks of AsO_4^{3-} appeared around 918-781 cm^{-1} (ν_3) and 425-419, 458-452, 511-490 cm^{-1} (ν_4). The hydroxyl-stretching region bands are resolved at 3444-3430, 3185-3150 and 3047-3021 cm^{-1}. The band at around 3444-3430 cm^{-1} is attributed to an AsOH stretching vibration. The two bands at 3185-3150 and 3047-3021 cm^{-1} are attributed to the OH stretching bands of water. Water bending modes are detected in the infrared spectrum at 1587-1403 cm^{-1}.

Well-crystallized solids are formed. All of the solid solution samples were observed by SEM to have a platy morphology of flattened striated blades or radiating acicular crystals (Fig. 3). The crystallininty of erythrite and annabergite is related to the synthetic procedure and condition[9,10]. Vigorous stirring of the nitrate solution was important to suppress the formation of gelatinous, poorly crystallized arsenate phase. The temperature

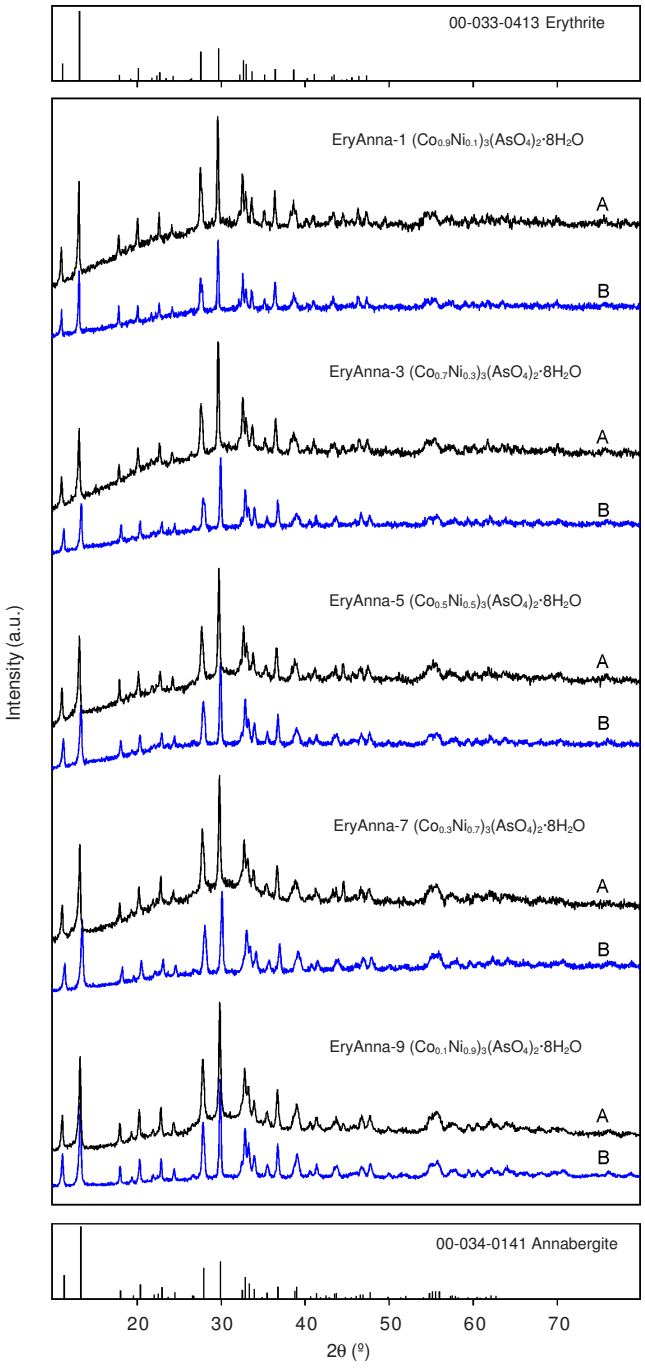

Fig. 1. X-ray diffraction patterns of the $(Co_xNi_{1-x})_3(AsO_4)_2{\cdot}8H_2O$ solid solutions before (A) and after (B) dissolution at 25 ºC for 2880 h

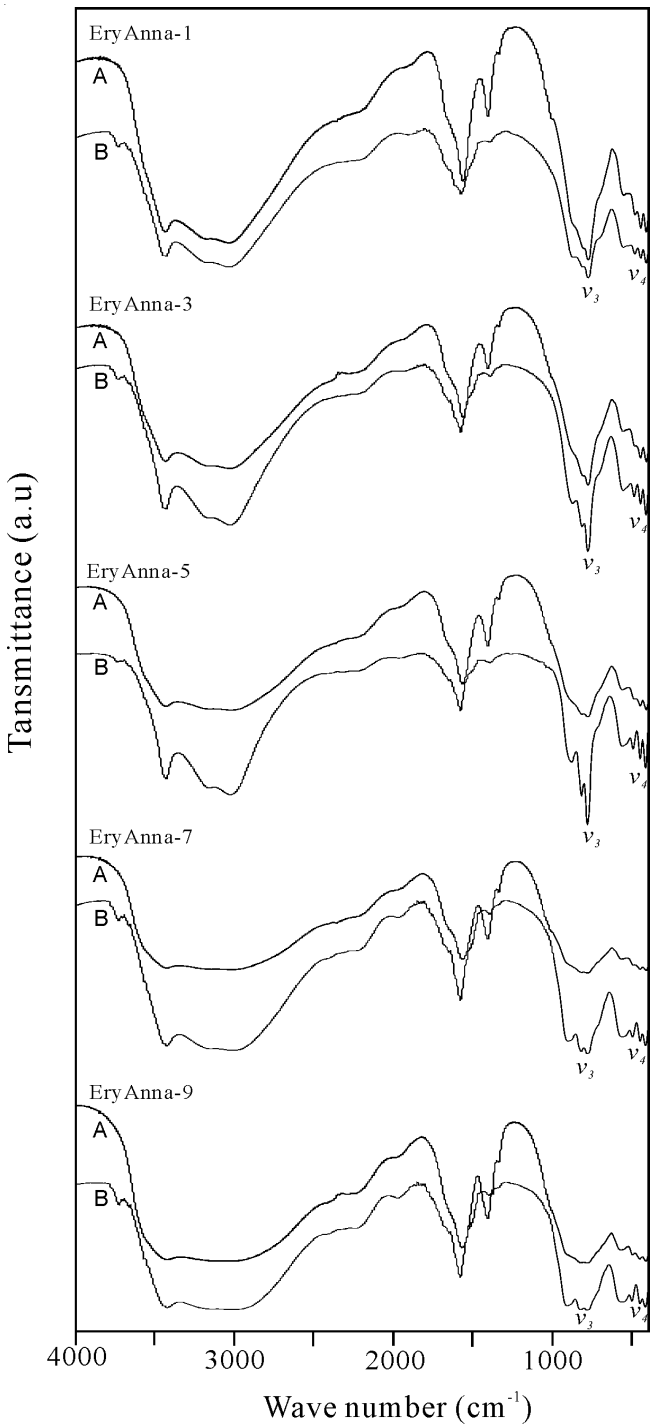

Fig. 2. Infrared spectra of the $(Co_xNi_{1-x})_3(AsO_4)_2{\cdot}8H_2O$ solid solutions before (A) and after (B) dissolution at 25 ºC for 2880 h

of the nitrate solution had little effect on the crystallinity of the precipitates.

Evolution of aqueous composition and dissolution mechanism: The solution pH and element concentrations during the dissolution experiments at 25 ºC and initial pH 2 as a function of time are shown in Fig. 4 for the erythrite/annabergite solid solution. The dissolution process of nine different solid solution samples was similar to each other. The experimental results indicated that the dissolution could be stoichiometrical only at the beginning of the process and then dissolution became non-stoichiometrical and the system

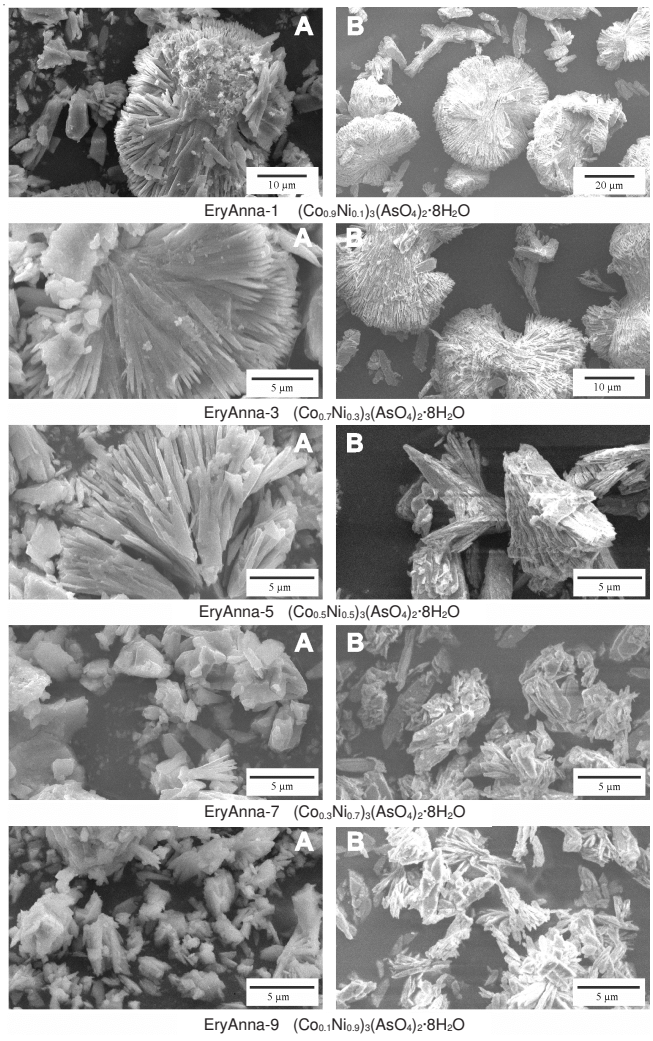

Fig. 3. Scanning electron micrographs of the $(Co_xNi_{1-x})_3(AsO_4)_2{\cdot}8H_2O$ solid solutions before (A) and after (B) dissolution at 25 ºC for 2880 h

underwent a dissolution-recrystallization process that affects the ratio of the substituting ions in both the solid and the aqueous solution. Dissolution of the erythrite/annabergite solid solution in aqueous medium appeared to be always non-stoichiometric at the atomic level in our experiments. During the dissolution (0-2880 h), the release of cobalt and nickel into the bulk solution was always less when compared with the release of arsenate, *i.e.*, the dissolution reaction was incongruent with arsenate being released to solution in stoichiometric excess of cobalt and nickel.

When dissolution progressed at the initial pH 2, the release rates of Co, Ni and arsenate rapidly increased until the peak values of the aqueous cobalt, nickel and arsenate concentrations were reached within 1 h reaction. And then the over-all dissolution rate of the erythrite/annabergite solid solution decreased while the aqueous (Co + Ni)/As atomic ratio varied between 0.22-2.26 (in total 198 data, only five points >1.5: 1.54, 1.72, 1.83, 1.85, 2.26), which is lower than the stoichiometric ratio of 1.50. After the dissolution for 48-72 h, the aqueous Co, Ni and As concentrations reached their minimum values. After that time, they increased gradually once again and finally approached a steady state. Accompanying the early release of Co, Ni and As was a rapid increase in

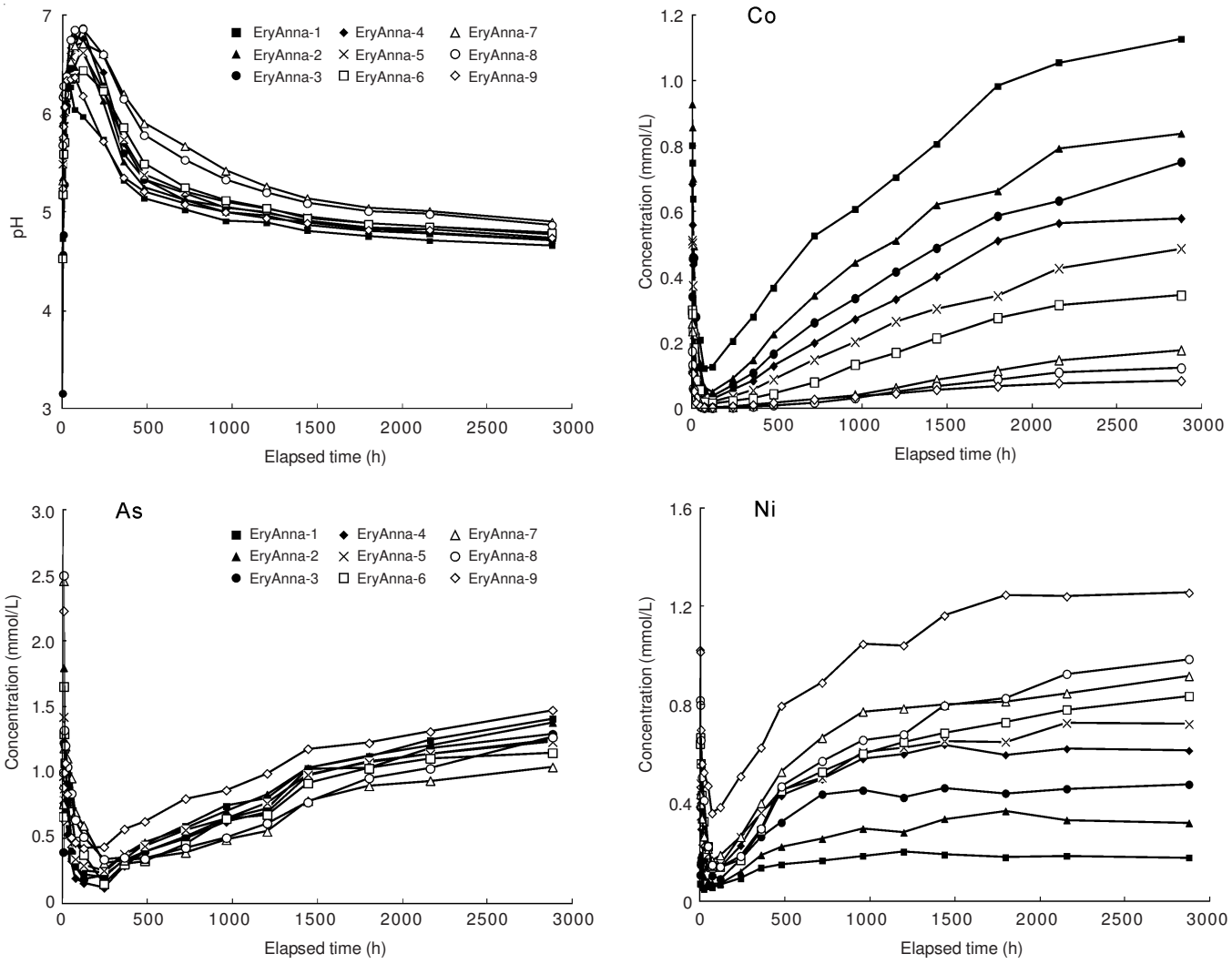

Fig. 4. Aqueous element concentrations *versus* time for dissolution of the $(Co_xNi_{1-x})_3(AsO_4)_2{\cdot}8H_2O$ solid solutions at 25 ºC

reacted solution pHs from 2 to 5.58-6.87 in the first 48-72 h of the dissolution experiment and then the solution pHs decreased gradually until they reached their steady state values of around 4.56-4.87. When an initial portion of the solid has been dissolved, the solution pHs increased rapidly because of the hydrolyzing reactions, which would cause the lower solubility of the minerals in the solution and a re-crystallization of the solid that resulted in a decreasing in the aqueous element concentrations.

During the early stages of the dissolution reaction, mineral components were released in non-stoichiometric ratios with reacted solution ratios of dissolved (Co + Ni)/As being smaller than mineral stoichiometric ratios of $X_3(AsO_4)_2{\cdot}8H_2O$, *i.e.*, 1.50. This suggests that As are being preferentially released from the mineral structure compared to Co or Ni. The reason is considered to be related to the dissolution of crystal edges and corners. When the edges and corners of erythrite and annabergite mainly consist of arsenate, the dissolution will start by chemical interaction of protons with these weakly bounded arsenate groups. This suggests that arsenate was preferentially released compared to Co and Ni from the mineral structure[9,10,18]. These results suggest that the composition of these final equilibrated solutions may be controlled by a surface layer having a composition distinct from that of the erythrite/annabergite solid solution. Because of the low solubility, they dissolution kinetics were controlled by chemical reactions occurring at the mineral surface[19,20].

In general, the aqueous concentrations of elements were strongly depended on the mole fraction of the endmember erythrite $[Co_3(AsO_4)_2{\cdot}8H_2O]$ and annabergite $[Ni_3(AsO_4)_2{\cdot}8H_2O]$ in the erythrite/annabergite solid solution. The final solution pH values and the concentrations of aqueous Co, Ni and arsenate species were strongly related to the mole fraction of erythrite $[Co_3(AsO_4)_2{\cdot}8H_2O]$ or annabergite $[Ni_3(AsO_4)_2{\cdot}8H_2O]$ in the solid samples (Fig. 5). Generally, the aqueous Co concentrations increased with the increase in the mole fraction of the endmember erythrite $[Co_3(AsO_4)_2{\cdot}8H_2O]$ in the erythrite/annabergite solid solution and the aqueous Ni concentrations increased with the increase in the mole fraction of the endmember annabergite $[Ni_3(AsO_4)_2{\cdot}8H_2O]$ in the solid solution. The erythrite/annabergite solid-solution had a minimum aqueous arsenate concentration or a minimum solubility at the mole fraction of erythrite in the erythrite/annabergite solid solution $[(Co_xNi_{1-x})_3(AsO_4)_2{\cdot}8H_2O]$ of 0.70 (Fig. 5). It is also obvious that the solution pH increased or the aqueous H^+ concentrations

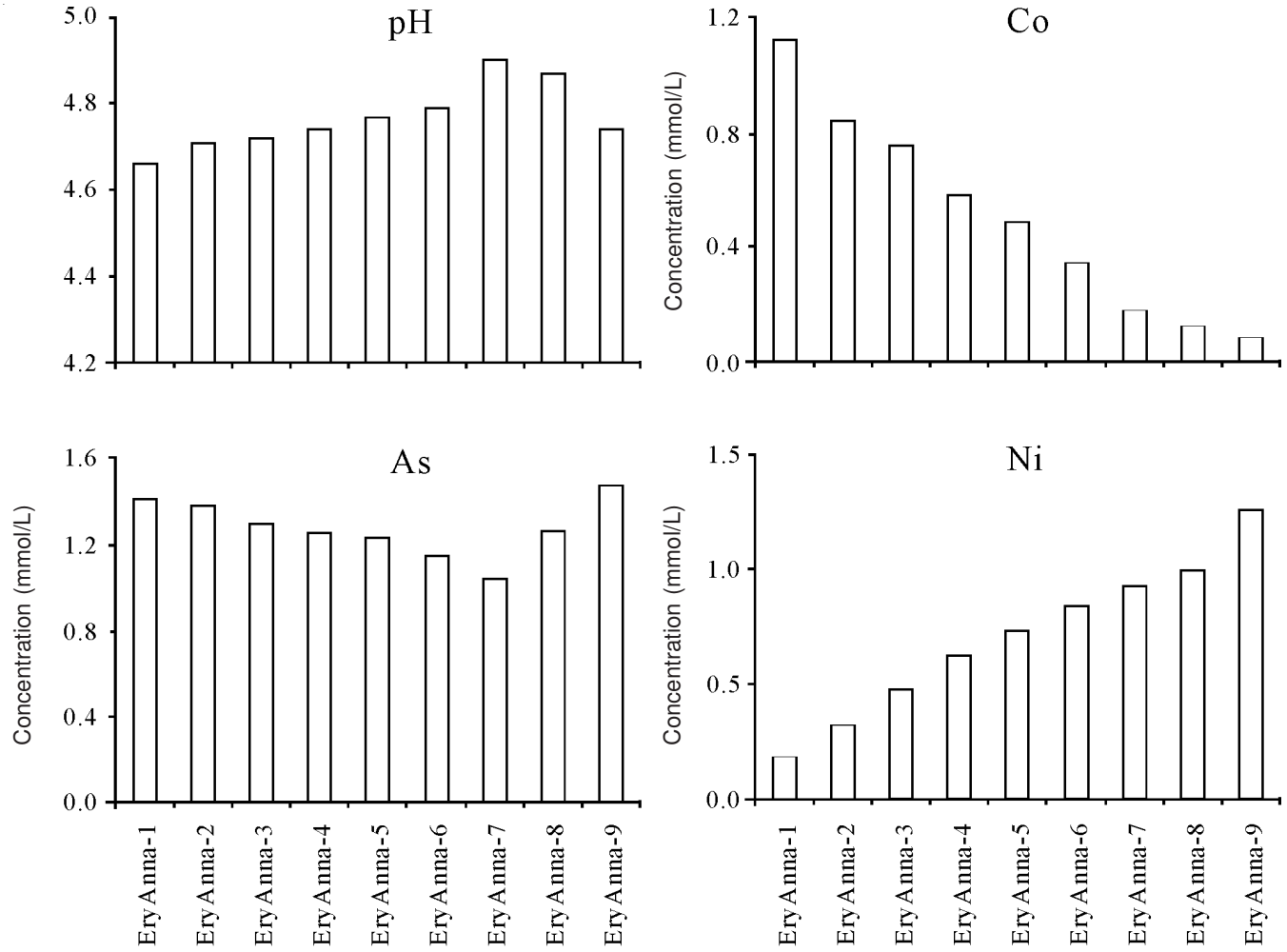

Fig. 5. Aqueous pH and the aqueous concentrations of elements after the dissolution of the $(Co_xNi_{1-x})_3(AsO_4)_2{\cdot}8H_2O$ solid solution for 2880 h

decreased with the increase in the concentrations of aqueous arsenate species (Fig. 5). This solubility behaviour is consistent with that of phase-pure erythrite $[Co_3(AsO_4)_2{\cdot}8H_2O]$ and annabergite $[Ni_3(AsO_4)_2{\cdot}8H_2O]$. Erythrite $[Co_3(AsO_4)_2{\cdot}8H_2O]$ and annabergite $[Ni_3(AsO_4)_2{\cdot}8H_2O]$ become more soluble at lower pH and less soluble at high pH.

The proton consumption suggested that adsorption of protons onto negatively charged oxygen ions of arsenate groups of the erythrite/annabergite solid solution had occurred. Sorption of protons would result in transformation of surface AsO_4^{3-} groups into $HAsO_4^{2-}$ which should catalyze the dissolution process[19]. Furthermore, the existence of both dissolution and exchange reactions implies that the protons consumed during the dissolution do not originate solely from sorption/desorption of protons but from several distinct reactions at the solid surface. A complete description of the protons consumed during the dissolution must, therefore, take account of the following reactions: stoichiometric dissolution of the bulk solid, stoichiometric exchange of $2H^+$ for one Co^{2+} or Ni^{2+} at the solid surface, H^+ adsorption/desorption on the solid surface.

The stoichiometric dissolution reaction of the bulk solid releases Co, Ni and As according to:

$$X_3(AsO_4)_2{\cdot}8H_2O = 3X^{2+} + 2AsO_4^{3-} + 8H_2O \quad (1)$$

where $X^{2+} = Co^{2+}$ or Ni^{2+}.

Liberated Co, Ni and As hydrolyze in solution according to:

$$X^{2+} + H_2O = XOH^+ + H^+ \quad (2)$$

$$AsO_4^{3-} + H^+ = HAsO_4^{2-} \quad (3)$$

$$AsO_4^{3-} + 2H^+ = H_2AsO_4^- \quad (4)$$

$$AsO_4^{3-} + 3H^+ = H_3AsO_4 \quad (5)$$

Within the investigated pH range of $5 < pH < 10$, only reactions (3) and (4) contribute significantly to the proton balance. This could be explained on the basis of the high dissociation constants of H_3AsO_4 ($K_1 = 4.0 \times 10^{-3}$, $K_2 = 1.0 \times 10^{-7}$ and $K_3 = 3.2 \times 10^{-12}$).

Current knowledge on arsenic chemistry may be distorted because information available on the solubility of arsenic compounds usually does not include possible formation of metal-arsenate complexes[16,17,21]. The possible formation of metal arsenate complexes could significantly affect the dissolution mechanism. Various authors have proposed the existence of these complexes[16,17,21], although the presence and the thermodynamic properties of the metal arsenate complexes need to be confirmed by further works[16,17]. The possible formation reactions of Co-arsenate and Ni-arsenate complexes could take the following forms:

$$Co^{2+} + AsO_4^{3-} = CoAsO_4^- \quad (6)$$

$$Co^{2+} + HAsO_4^{2-} = CoHAsO_4 \quad (7)$$

$$Co^{2+} + H_2AsO_4^- = CoH_2AsO_4^+ \quad (8)$$

$$Ni^{2+} + AsO_4^{3-} = NiAsO_4^- \quad (9)$$

$$Ni^{2+} + HAsO_4^{2-} = NiHAsO_4 \quad (10)$$

$$Ni^{2+} + H_2AsO_4^- = NiH_2AsO_4^+ \quad (11)$$

After 1 h of the dissolution at initial pH 2, the calculation with PHREEQC indicated that the dissolved cobalt existed mainly as Co^{2+} (96.57-98.91 %) and $CoHAsO_4$ (< 2.26 %); the dissolved nickel existed mainly as Ni^{2+} (94.36-98.25 %), $NiHAsO_4$ (<1.31 %) and $NiH_2AsO_4^+$ (< 2.44 %); the dissolved arsenate existed mainly as $H_2AsO_4^-$ (86.79-97.96 %) and $HAsO_4^{2-}$ (0.03-9.50 %) in the solution. The overall dissolution reaction may be predominantly described by the chemical mechanism (1) and (4). And a very small amount of the metal arsenate complexes $CoHAsO_4$, $NiHAsO_4$ and $NiH_2AsO_4^+$ could form in solution through the reactions (7), (10) and (11).

After 48 h of the dissolution at initial pH 2, the calculation with PHREEQC indicated that the dissolved cobalt existed mainly as Co^{2+} (86.60-98.67 %) and $CoHAsO_4$ (<10.85 %); the dissolved nickel existed mainly as Ni^{2+} (79.32-95.26 %), $NiHAsO_4$ (< 5.82 %) and $NiH_2AsO_4^+$ (< 0.91 %); the dissolved arsenate existed mainly as $H_2AsO_4^-$ (42.59-92.17 %) and $HAsO_4^{2-}$ (7.30-52.07 %) in the solution. The overall dissolution reaction may be predominantly described by the chemical reactions (1), (3) and (4). And some amount of the metal arsenate complexes $CoHAsO_4$ and $NiHAsO_4$ formed in solution through the reactions (7) and (10).

After 2880 h of the dissolution at initial pH 2, the calculation with PHREEQC indicated that the dissolved cobalt existed mainly as Co^{2+} (99.05-99.30 %) and $CoHAsO_4$ (< 0.53 %); the dissolved nickel existed mainly as Ni^{2+} (95.46-96.32 %) with $NiHAsO_4$ (< 0.30 %) and $NiH_2AsO_4^+$ (< 3.52 %); the dissolved arsenate existed mainly as $H_2AsO_4^-$ (93.26-98.41 %) and $HAsO_4^{2-}$ (0.76-1.51 %) in the solution. The overall dissolution reaction may be predominantly described by the chemical mechanism (1) and (4). And a small amount of the metal arsenate complexes $NiH_2AsO_4^+$ could form in solution through the reaction (11).

Saturation index for erythrite and annabergite: The thermodynamic analysis could be initiated by assuming the possible pure-phase equilibrium relations[22]. Pure-phase equilibrium was assessed by calculating the saturation index (SI), defined by $SI = \log IAP/K_{sp}$. Where IAP is the ion activity product (*i.e.*, $[Co^{2+}]^3[AsO_4^{3-}]^2$ or $[Ni^{2+}]^3[AsO_4^{3-}]^2$) and the solubility product K_{sp} is the thermodynamic-equilibrium constant for the dissolution reaction. If the SI is equal to zero, the aqueous phase is in equilibrium with the solid phase. A SI greater than zero indicates supersaturation and a SI lesser than zero indicates undersaturation.

Erythrite $[Co_3(AsO_4)_2{\cdot}8H_2O]$ is less soluble than annabergite $[Ni_3(AsO_4)_2{\cdot}8H_2O]$. The mean K_{sp} values were calculated for erythrite $[Co_3(AsO_4)_2{\cdot}8H_2O]$ of $10^{-34.02}$ ($10^{-33.53}$-$10^{-34.68}$) at 25 ºC, for annabergite $[Ni_3(AsO_4)_2{\cdot}8H_2O]$ of $10^{-30.77}$ ($10^{-29.83}$-$10^{-32.57}$) at 25 ºC[22]. The K_{sp} value of $10^{-34.02}$ for erythrite is similar to the K_{sp} value of $10^{-32.35}$ reported by Lee and Nriagu[21], but it is approximately 5.23-5.90 log units smaller than that of $10^{-28.796}$ determined by Nishimura *et al.*[23] and that of $10^{-28.119}$ reported in literature given by Chukhlantsev[24] and Martens *et al.*[18]. The K_{sp} value of $10^{-30.77}$ for annabergite is approximately 2.39-5.05 log units smaller than the obtained K_{sp} values of $10^{-25.721}$ obtained by Chukhlantsev[24] and Martens *et al.*[18], $10^{-28.380}$ obtained by Nishimura *et al.*[23] and $10^{-27.290}$ obtained by Essington[25].

These discrepant solubility products can be due to differences between the minerals in the different studies, but also due to differences in the way the experiments in the studies have been conducted. Inconsistency in data presented in literature could also be due to the failure to achieve equilibrium. The classic work on arsenate solubility is often referred in the work of Chukhlantsev[24]. The conditional solubility product constants were not corrected for ionic strength and determined at 20 ºC. All thermodynamic data compilations that consider metal arsenates, principally geochemical model data bases, contain the stability product constant determined by Chukhlantsev[24], converted to zero ionic strength and 25 ºC. Martens *et al.*[18] cited the K_{sp} data of erythrite and annabergite without giving their original experimental data or their source. Langmuir *et al.*[26] determined the solubility of annabergite based not on their own experimental measurement, but on the data of Nishimura *et al.*[23].

Therefore, the K_{sp} values of $10^{-34.02}$ for erythrite and $10^{-30.77}$ for annabergite were used in the calculation using the program PHREEQC in the present study. The calculated saturation indices for erythrite $[Co_3(AsO_4)_2{\cdot}8H_2O]$ show a trend of increasing values as the composition of the solid phases approaches that of the pure-phase endmember, $[Co_3(AsO_4)_2{\cdot}8H_2O]$ (Fig. 6). At the beginning of the dissolution of the $(Co_xNi_{1-x})_3(AsO_4)_2{\cdot}8H_2O$ solid solutions, the $Co_3(AsO_4)_2{\cdot}8H_2O$ saturation index (SI) values increased with time until the aqueous solution was oversaturated with respect to $Co_3(AsO_4)_2{\cdot}8H_2O$ and then the SI values decreased slowly. At the end of the dissolution experiment (2880 h), the aqueous solution was saturated with respect to $Co_3(AsO_4)_2{\cdot}8H_2O$ for the $(Co_xNi_{1-x})_3(AsO_4)_2{\cdot}8H_2O$ solid solutions with $x \geq 0.5$, while the aqueous solution was undersaturated with respect to $Co_3(AsO_4)_2{\cdot}8H_2O$ for the $(Co_xNi_{1-x})_3(AsO_4)_2{\cdot}8H_2O$ solid solutions with $x < 0.5$.

The calculated saturation indices for annabergite $[Ni_3(AsO_4)_2{\cdot}8H_2O]$ show a distinctly different trend than those for erythrite $[Co_3(AsO_4)_2{\cdot}8H_2O]$ (Fig. 6). Generally, the $Ni_3(AsO_4)_2{\cdot}8H_2O$ saturated index (SI) values decreased as the $Ni_3(AsO_4)_2{\cdot}8H_2O$ mole fraction decreased or the $Co_3(AsO_4)_2{\cdot}8H_2O$ mole fraction increased. At the beginning of the dissolution, the $Ni_3(AsO_4)_2{\cdot}8H_2O$ saturated index (SI) values increased with time until the aqueous solution was oversaturated with respect to $Ni_3(AsO_4)_2{\cdot}8H_2O$ and then the SI values decreased slowly. At the end of the dissolution experiment (2880 h), the aqueous solution was saturated with respect to $Ni_3(AsO_4)_2{\cdot}8H_2O$ for the $(Co_xNi_{1-x})_3(AsO_4)_2{\cdot}8H_2O$ solid solutions with $x \leq 0.3$, while the aqueous solution was undersaturated with respect to $Ni_3(AsO_4)_2{\cdot}8H_2O$ for the $(Co_xNi_{1-x})_3(AsO_4)_2{\cdot}8H_2O$ solid solutions with $x > 0.3$.

The saturation indexes were also calculated using PHREEQC with respect to cobalt and nickel compounds other than erythrite and annabergite. The results indicated that all aqueous solutions were always undersaturated with respect to any other potential secondary phases, *e.g.*, CoO, $Co(OH)_2$, NiO and $Ni(OH)_2$, with the SI of -10.91 ~ -4.44, -10.41 ~ -3.94, -10.26 ~ -2.79 and -10.60 ~ -3.13, respectively. For all aqueous solution samples, the saturation indexes with respect to $NiHAsO_4$ were calculated to be -21.40 ~ -13.34.

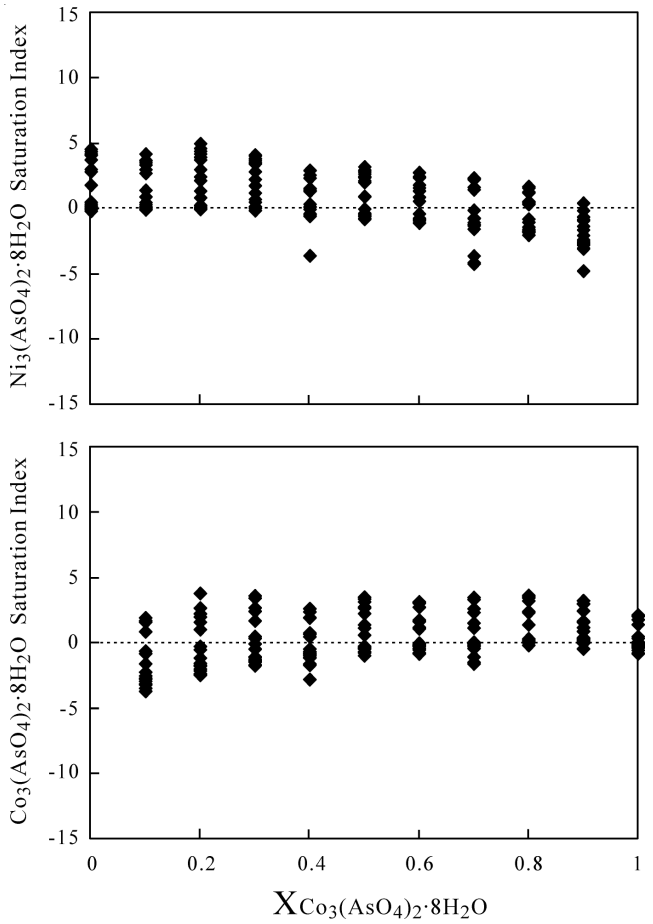

Fig. 6. Calculated saturation indices for erythrite [$Co_3(AsO_4)_2{\cdot}8H_2O$] and annabergite [$Ni_3(AsO_4)_2{\cdot}8H_2O$]

Construction of Lippmann diagram: Understanding about the solid solution-aqueous solution processes is of fundamental importance. However, in spite of the numerous studies, the availability of thermodynamic data for solid solution-aqueous solution systems is still scarce[27]. Lippmann extended the solubility product concept to solid solutions by developing the concept of "total activity product" $\Sigma\pi_{SS}$, which is defined as the sum of the partial activity products contributed by the individual endmembers of the solid solution[27,28]. At thermodynamic equilibrium, the total activity product $\Sigma\pi_{eq}$, expressed as a function of the solid composition, yields the Lippmann's "*solidus*" relationship. In the same way, the "*solutus*" relationship expresses $\Sigma\pi_{eq}$ as a function of the aqueous solution composition. The graphical representation of "*solidus*" and "*solutus*" yields a phase diagram, usually known as a Lippmann diagram[27,28]. A comprehensive methodology for describing reaction paths and equilibrium end points in solid-solution aqueous solution systems had been presented and discussed in literatures[22,28-30].

When there are several sites per formula unit for the substituting ions, the relationship between the activities of the components and the molar fractions of the substitution ions can be simplified by considering the chemical formula on a "one-substituting-ion" basis. In the case of the erythrite/annabergite solid solution [$(Co_xNi_{1-x})_3(AsO_4)_2{\cdot}8H_2O$] (EryAnna), the formula units of the components are redefined as $Co(AsO_4)_{2/3}{\cdot}^8/_3H_2O$ ($Ery_{1/3}$) and $Ni(AsO_4)_{2/3}{\cdot}^8/_3H_2O$ ($Anna_{1/3}$), which is equivalent to consider the formula unit of the solid solution as $(Co_xNi_{1-x})(AsO_4)_{2/3}{\cdot}^8/_3H_2O$ ($EryAnna_{1/3}$). A simple justification of this relation lies in the expression for the configurational entropy of mixing, which can be derived from the Boltzmann relation[31], assuming the simplest possible model for the distribution of atoms, namely that these are distributed randomly in the solid solution within their structural sites[32]. A Lippmann diagram is based on the total solubility product, $\Sigma\pi$, which for the $(Co_xNi_{1-x})(AsO_4)_{2/3}{\cdot}^8/_3H_2O$ solid solution ($EryAnna_{1/3}$) can be written as:

$$\Sigma\pi_{EryAnna_{1/3}} = ([Co^{2+}]+[Ni^{2+}])[AsO_4^{3-}]^{2/3}$$
$$= K_{Ery_{1/3}}X_{Ery1/3}\gamma_{Ery_{1/3}} + K_{Anna_{1/3}}X_{Anna_{1/3}}\gamma_{Anna_{1/3}} \quad (12)$$

where [] designate aqueous activity. $K_{Ery_{1/3}}$ and $K_{Anna_{1/3}}$, $X_{Ery1/3}$ and $X_{Anna_{1/3}}$, $\gamma_{Ery_{1/3}}$ and $\gamma_{Anna_{1/3}}$ are the thermodynamic solubility products, the mole fractions (x, 1-x) and the activity coefficients of the $Co(AsO_4)_{2/3}{\cdot}^8/_3H_2O$ ($Ery_{1/3}$) and $Ni(AsO_4)_{2/3}{\cdot}^8/_3H_2O$ ($Anna_{1/3}$) components in the $(Co_xNi_{1-x})(AsO_4)_{2/3}{\cdot}^8/_3H_2O$ ($EryAnna_{1/3}$) solid solution. The term $([Co^{2+}]+[Ni^{2+}])[AsO_4^{3-}]^{2/3}$ is the "total solubility product $\Sigma\pi_{EryAnna_{1/3}}$" at equilibrium[28]. This relationship, called the *solidus*, defines all possible thermodynamic saturation states for the two-component solid solution series in terms of the solid phase composition[32].

As given by Glynn and Reardon[28], the equation of the solutus can be given by:

$$\Sigma\pi_{EryAnna_{1/3}} = \frac{1}{\frac{X_{Co^{2+},aq}}{K_{Ery_{1/3}}\gamma_{Ery_{1/3}}} + \frac{X_{NI^{2+},aq}}{K_{Anna_{1/3}}\gamma_{Anna_{1/3}}}} \quad (13)$$

where $X_{Co^{2+},aq}$ and $X_{Ni^{2+},aq}$ are the activity fractions for $[Co^{2+}]$ and $[Ni^{2+}]$ in the aqueous phase, respectively. This relationship defines all possible thermodynamic saturation states for the two-component solid solution series in terms of the aqueous phase composition[32].

Identical to the equation for the solid solution curves given by Glynn and Reardon[28], the total solubility product for the $(Co_xNi_{1-x})(AsO_4)_{2/3}{\cdot}^8/_3H_2O$ solid solution at stoichiometric saturation, $\Sigma\pi_{SS}$, can be expressed as:

$$\Sigma\pi_{SS} = \frac{K_{SS}}{(X_{Co^{2+},aq})^{X_{Ery1/3}}(X_{Ni^{2+},aq})^{X_{Anna1/3}}} \quad (14)$$

where K_{SS}, $[Co^{2+}]^x[Ni^{2+}]^{(1-x)}[AsO_4^{3-}]^{2/3}$, is the stoichiometric saturation constant for the $(Co_xNi_{1-x})(AsO_4)_{2/3}{\cdot}^8/_3H_2O$ solid solution.

The total solubility products for the stoichiometric saturation with respect to both pure endmembers, $\Sigma\pi_{Ery_{1/3}}$ and $\Sigma\pi_{Anna_{1/3}}$, can be described in terms of the endmember solubility products $K_{Ery_{1/3}}$ and $K_{Anna_{1/3}}$, respectively:

$$\Sigma\pi_{Ery_{1/3}} = \frac{[Co^{2+}][AsO_4^{3-}]^{2/3}}{(X_{Co^{2+},aq})^{X_{Ery1/3}}} = \frac{K_{Ery1/3}}{(X_{Co^{2+},aq})^{X_{Ery1/3}}} \quad (15)$$

$$\Sigma\pi_{Anna_{1/3}} = \frac{[Ni^{2+}][AsO_4^{3-}]^{2/3}}{(X_{Ni^{2+},aq})^{X_{Anna1/3}}} = \frac{K_{Anna1/3}}{(X_{Ni^{2+},aq})^{X_{Anna1/3}}} \quad (16)$$

According to the definition of the total solubility product, the "total solubility product $\Sigma\pi_{EryAnna}$" for the formula unit of

the solid solution as $(Co_xNi_{1-x})_3(AsO_4)_2{\cdot}8H_2O$ can be calculated from the "total solubility product $\Sigma\pi_{EryAnna_{1/3}}$" by:

$$\Sigma\pi_{EryAnna} = ([Co^{2+}]+[Ni^{2+}])^3[AsO_4^{3-}]^2 = \{([Co^{2+}]+[Ni^{2+}])[AsO_4^{3-}]^{2/3}\}^3 = \{\Sigma\pi_{EryAnna_{1/3}}\}^3 \quad (17)$$

A Lippmann phase diagram for the solid solution as $(Co_xNi_{1-x})_3(AsO_4)_2{\cdot}8H_2O$ is a plot of the solidus and *solutus* as log $\Sigma\pi_{EryAnna}$ (or log$\{\Sigma\pi_{EryAnna}\}^3$) on the ordinate *versus* two superimposed aqueous and solid phase mole fraction scales on the abscissa.

Solid-solution aqueous-solution reaction paths: The solid-solution excess free energy and the two Guggenheim parameters a_o and a_1 can be determined from a given alyotropic composition and alyotropic solubility, which is performed in MBSSAS, a code for the computation of Margules parameters and equilibrium relations in binary solid-solution aqueous-solution systems. An alyotropic composition can be defined as an intermediate composition for which a solid solution has a minimum solubility[33]. In the present experimental data, the erythrite-annabergite solid-solution had a minimum solubility at the mole fraction of erythrite in the solid solution of 0.70 (Fig. 5). In respect to the $(Co_xNi_{1-x})(AsO_4)_{2/3}{\cdot}^8/_3H_2O$ solid solution, the corresponding log $\Sigma\pi$ value of the alyotropic extremum was calculated from the aqueous Co, Ni and As concentrations to be -11.21. The a_o and a_1 parameters were then determined to be -1.79 and 1.23, respectively.

A Lippmann diagram for the erythrite-annabergite solid solution for the ideal case when $a_0 = 0.0$ and for the non-ideal case when $a_0 = -1.79$ and $a_1 = 1.23$ is shown in Fig. 7. It was constructed using thermodynamic solubility products for erythrite of $10^{-33.68}$ and annabergite of $10^{-32.34}$ reported in the previous researches. The diagrams contain the solidus (log $\Sigma\pi_{EryAnna}$ *vs.* $X_{Ery_{1/3}}$ or X_{Ery}) and the solutus (log $\Sigma\pi_{EryAnna}$ *vs.* $X_{Co^{2+},aq}$) for the erythrite/annabergite solid solution and the total solubility product curve at stoichiometric saturation for the erythrite-annabergite solid solution at x = 0.50. In addition to the *solutus* and the solidus, the saturation curves for pure endmembers erythrite (x = 1.00) and annabergite (x = 0.00) have also been plotted in the chart. Also included are the data from our study, plotted as $([Co^{2+}]+[Ni^{2+}])^3[AsO_4^{3-}]^2$ *vs.* $X_{Co^{2+},aq}$.

If the endmember solubility products are close, the solutes is in equilibrium with a much more evenly distributed range of solid compositions and the solutus and solidus curves plot near each other[28]. In the $(Co_xNi_{1-x})_3(AsO_4)_2{\cdot}8H_2O$ system, the endmember solubility products differ by about 1.34 log $\Sigma\pi_{EryAnna}$ or 0.45 log $\Sigma\pi_{EryAnna}$. The $(Co_xNi_{1-x})_3(AsO_4)_2{\cdot}8H_2O$ solid solutions are assumed ideal. In this case, the pure-phase solubility curves for erythrite and annabergite are quite distinct from the solutus and the solution compositions along the solutus are clearly undersaturated with respect to both pure erythrite and pure annabergite solids.

The solutus and solidus curves of the $(Co_xNi_{1-x})_3(AsO_4)_2{\cdot}8H_2O$ system with $a_0 = -1.79$ and $a_1 = 1.23$ are also illustrated in the figure. Because a negative excess free energy lowers the position of the solutus curve relative to the position of an ideal solutus, the solutus in this case lies distinctly below the pure phase saturation curves[28]. The system also shows an alyotropic minimum, a point of intermediate composition corresponding to a minimum in the solidus curve at $X_{Ery} = 0.7$. The alyotropic minimum is a result of strong attraction between the two components of the solid solution[28].

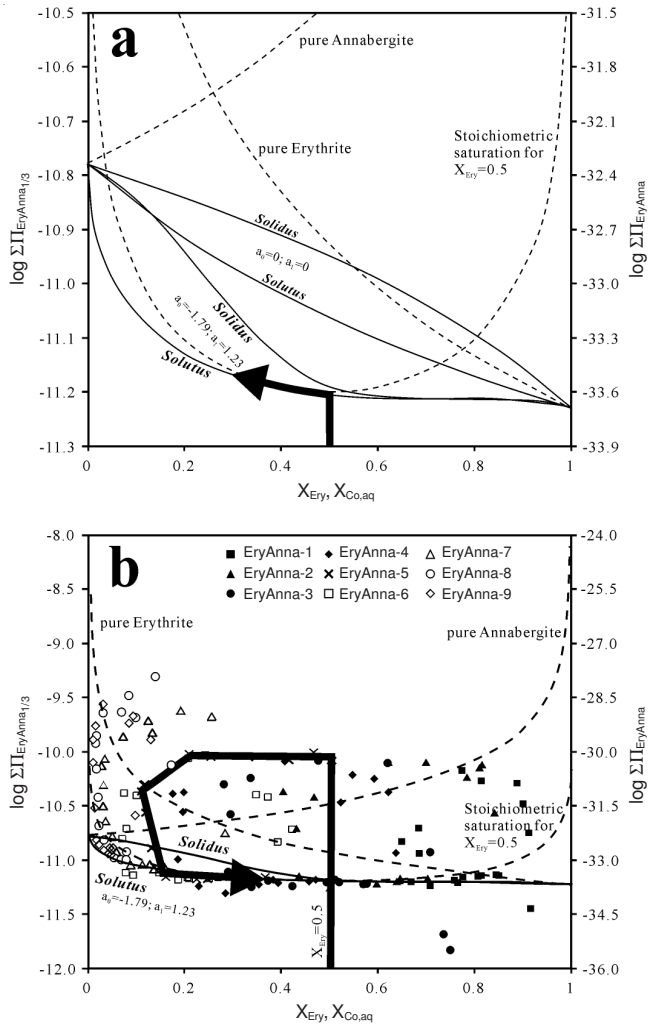

Fig. 7. Lippmann diagrams for dissolution of the erythrite/annabergite solid solutions $[(Co_xNi_{1-x})_3(AsO_4)_2{\cdot}8H_2O]$ showing possible stoichiometric dissolution pathway. (a) Hypothetical partial-equilibrium reaction path for the dissolution of the solid phase $(Co_{0.5}Ni_{0.5})_3(AsO_4)_2{\cdot}8H_2O$ is drawn in dark gray and arrowed lines. (b) Plotting of the experimental data on Lippmann diagrams with different abscissa. Solid arrows show the aqueous evolution with time in SSAS interaction

The hypothetical reaction path is also shown in Fig. 7a, in relation to Lippmann solutus and solidus curves for the $(Co_{0.5}Ni_{0.5})_3(AsO_4)_2{\cdot}8H_2O$ solid solution. The reaction path of a stoichiometrically dissolving solid solution moves vertically from the abscissa of a Lippmann diagram, originating at the mole fraction corresponding to the initial solid solution composition[32]. The pathway shows initial stoichiometric dissolution up to the solutus curve, followed by non-stoichiometric dissolution along the solutus, towards the more soluble endmember.

In general, the location of data points on a Lippmann diagram will depend on the aqueous speciation, degree to which secondary phases are formed and the relative rates of dissolution and precipitation[30]. As $(Co_xNi_{1-x})_3(AsO_4)_2{\cdot}8H_2O$ dissolves in solution, aqueous Co^{2+} is converted into $Co(OH)^+$, $Co(OH)_2$, $Co(OH)_3^-$, $Co(OH)_4^{2-}$, $Co_2OH_3^+$, $Co_4(OH)_4^{4+}$, $CoOOH^-$ and $CoNO_3^+$ as well as aqueous Ni^{2+} is converted into $NiOH^+$,

$Ni(OH)_2$, $Ni(OH)_3^-$ and $NiNO_3^+$, aqueous AsO_4^{3-} is converted primarily into $HAsO_4^{2-}$, $H_2AsO_4^-$ and H_3AsO_4, only a fraction remains as Co^{2+}, Ni^{2+} and AsO_4^{3-}. The smaller values of the activity fractions are a consequence of the Co^{2+} and Ni^{2+} speciation. For the plot of the experimental data on the Lippmann diagram, the effect of the aqueous Co^{2+} and Ni^{2+} speciation was considered by calculating the activity of Co^{2+} and Ni^{2+} with the program PHREEQC.

The experimental data plotted on Lippmann phase diagrams show that the $(Co_{0.5}Ni_{0.5})_3(AsO_4)_2{\cdot}8H_2O$ precipitate dissolved stoichiometrically at the beginning and approached to the Lippmann solutus curve and then overshoot the Lippmann solutus curve, the stoichiometric saturation curve for x = 0.50, the saturation curves for pure endmembers erythrite and annabergite. After the 3-6 h dissolution, the aqueous solution was oversaturated with respect to the $(Co_{0.5}Ni_{0.5})_3(AsO_4)_2{\cdot}8H_2O$ solid solution, erythrite and annabergite. And then, the $X_{Co,aq}$ decreased from 0.5 to 0.11 in 6-120 h with no obvious change in the log $\Sigma\pi_{EryAnna}$ value, indicating the dissolution path for this precipitate may involve stoichiometric dissolution to and overshot the Lippmann solutus curve followed by a possible exchange and recrystallization reaction. From 6 to120 h, the log $\Sigma\pi_{EryAnna}$ value decreased further, but the $X_{Co,aq}$ increased from 0.11 to about 0.37 and the dissolution approached and followed the solutus curve once again. The large difference between the solubility products of the endmembers involves a strong preferential partitioning of the less soluble endmember towards the solid phase. Our dissolution data indicate a final enrichment in the erythrite component in the solid phase and a persistent enrichment in the Ni^{2+} component in the aqueous phase (Table-1 and Fig. 7). The possibility of formation of a phase close in composition to pure erythrite seems unavoidable, given the lower solubility of erythrite and the large oversaturation with respect to erythrite, the relatively high solubility of annabergite and the undersaturation with respect to annabergite (Fig. 7).

Conclusion

Nine different members of the erythrite/annabergite solid solution $[(Co_xNi_{1-x})_3(AsO_4)_2{\cdot}8H_2O]$ were prepared and characterized by various techniques and then dissolution of the synthetic solids was studied at 25 ºC and pH 2 in a series of batch experiments for 2880 h. The XRD, FT-IR and SEM analyses indicated that the synthetic erythrite/annabergite solid solutions were found to have no obvious variation after dissolution. During the dissolution (0-2880 h), the release of cobalt or nickel into the bulk solution was always less when compared with release of arsenate. Generally, the aqueous Co or Ni concentrations increased with the increase in the mole fraction of $Co_3(AsO_4)_2{\cdot}8H_2O$ or $Ni_3(AsO_4)_2{\cdot}8H_2O$] in the solid solution, respectively. The erythrite/annabergite solid-solution $[(Co_xNi_{1-x})_3(AsO_4)_2{\cdot}8H_2O]$ had a minimum aqueous arsenate concentration or a minimum solubility at the mole fraction of erythrite in the solid solution of x = 0.70. The two Guggenheim parameters a_o and a_1 were determined to be -1.79 and 1.23 from the alyotropic composition and alyotropic solubility at x = 0.7. The Lippmann diagram for the erythrite-annabergite solid solution for the ideal case when $a_0 = 0.0$ and for the non-ideal case when $a_0 = -1.79$ and $a_1 = 1.23$ was constructed using thermodynamic solubility products for erythrite of $10^{-33.68}$ and annabergite of $10^{-32.34}$. The experimental data were plotted on Lippmann phase diagrams to show the evolution of the aqueous composition during the dissolution of the erythrite/annabergite solid solution.

ACKNOWLEDGEMENTS

The authors thank for the financial supports from the National Natural Science Foundation of China (41263009 and 40773059) and the Provincial Natural Science Foundation of Guangxi (2011GXNSFF018003, 2012GXNSFDA053022 and GuiKeZhong 1298002-3).

REFERENCES

1. E. Fulladosa, J.C. Murat, M. Martinez and I. Villaescusal, *Arch. Environ. Contam. Toxicol.*, **46**, 176 (2004).
2. M.A. Khan and Y.-S. Ho, *Asian J. Chem.*, **23**, 1889 (2011).
3. Y.J. Lee, P.W. Stephens, Y. Tang, W. Li, B.L. Phillips, J.B. Parise and R.J. Reeder, *Am. Mineral.*, **94**, 666 (2009).
4. T. Itakura, R. Sasai and H. Itoh, *J. Hazard. Mater.*, **146**, 328 (2007).
5. P.A. O'Day, *Elements*, **2**, 77 (2006).
6. J.L. Jambor and J.E. Dutrizac, *Can. Mineral.*, **33**, 1063 (1995).
7. B.M. Petrunic, A. Tom, L. Weaver and D. Hall, *Appl. Geochem.*, **24**, 2222 (2009).
8. P. Drahota and M. Filippi, *Environ. Int.*, **35**, 1243 (2009).
9. R.L. Frost, T. Kloprogge, M.L. Weier, W.N. Martens, Z. Ding and H.G.H. Edwards, *Spectrochim. Acta A*, **59**, 2241 (2003).
10. R.L. Frost, M.L. Weier, W.N. Martens, J.T. Kloprogge and Z. Ding, *Thermochim. Acta*, **403**, 237 (2003).
11. J.B. Percival, Y.T.J. Kwong, C.G. Dumaresq and F.A. Michel, In Proceedings of Mining and the Environment IV Conference, Sudbury, Ontario, Canada, pp.1-10 (2007).
12. U. Becker and M. Prieto, *Chem. Geol.*, **225**, 173 (2006).
13. J.V. Bothe Jr. and P.W. Brown, *Environ. Sci. Technol.*, **33**, 3806 (1999).
14. J.V. Bothe and P.W. Brown, *J. Hazard. Mater.*, **69**, 197 (1999).
15. D.L. Parkhurst and C.A.J. Appelo, User's Guide to PHREEQC (Version 2) - A Computer Program for Speciation, Reaction-Path, Advective-Transport and Inverse Geochemical Calculations, USGS Water-Resources Investigations Report, pp. 99-4259 (1999).
16. L. Marini and M. Accornero, *Environ. Geol.*, **52**, 1343 (2007).
17. L. Marini and M. Accornero, *Environ. Earth Sci.*, **59**, 1601 (2010).
18. W.N. Martens, J.T. Kloprogge, R.L. Frost and L. Rintoul, *Can. Mineral.*, **43**, 1065 (2005).
19. Y.N. Zhu, X.H. Zhang, H.H. Zeng, H.L. Liu, N. He and M.F. Qian, *Environ. Chem. Lett.*, **9**, 339 (2011).
20. R.A. Berner, *Rev. Mineral*, **8**, 111 (1981).
21. J.S. Lee and J.O. Nriagu, *Environ. Chem.*, **4**, 123 (2007).
22. A.R. Felmy, D. Rai and D.A. Moore, *Geochim. Cosmochim. Acta*, **57**, 4345 (1993).
23. T. Nishimura, C.T. Itoh and K. Tozawa, in eds.: R.G. Reddy, J.L. Hendrix and P.B. Queneau, Arsenic Metallurgy Fundamentals and Applications, TMS, Warrendale PA, 77 (1988).
24. V.G. Chukhlantsev, *J. Inorg. Chem.*, **1**, 1975 (1956) (in Russian).
25. M.E. Essington, *Soil Sci. Soc. Am. J.*, **52**, 1566 (1988).
26. D. Langmuir, J. Mahoney, A. MacDonald and J. Rowson, *Geochim. Cosmochim. Acta*, **63**, 3379 (1999).
27. M. Prieto, *Rev. Mineral. Geochem.*, **70**, 47 (2009).
28. P.D. Glynn and E.J. Reardon, *Am. J. Sci.*, **290**, 164 (1990).
29. C. Monnin, *Chem. Geol.*, **153**, 187 (1999).
30. D. Baron and C.D. Palmer, *Geochim. Cosmochim. Acta*, **66**, 2841 (2002).
31. J. Ganguly and S.K. Saxena, Mixtures and Mineral Reactions, Springer-Verlag, Berlin and New York, pp. 1-291 (1987).
32. W.A. Kornicker, P.A. Presta, C.A. Paige, D.M. Johnson, O.E. Hileman and W.J. Snodgrass, *Geochim. Cosmochim. Acta*, **55**, 3531 (1991).
33. F. Lippmann, *Neues Jb. Miner. Abh.*, **139**, 1 (1980).